High-Brightness Plasmon-Enhanced Nanostructured Gold Photoemitter

Y. Gong, Alan G. Joly, L. M. Kong, Patrick Z. El-Khoury, and Wayne P. Hess*

Pacific Northwest National Laboratory, Physical Sciences Division, P. O. Box 999, Richland, Washington 99352, USA

(Received 29 January 2014; revised manuscript received 30 June 2014; published 30 December 2014)

We fabricate plasmonic nanohole arrays in gold thin films by focused-ion-beam lithography. Subsequent heat treatment of the lithographic patterns induces the growth of sub-100-nm structures including tips, rods, and flakes, all localized in the nanohole-array region. The coupled nanohole-array–nanostructure system comprises an efficient photoemitter. High-brightness photoemission is observed from this construct, following 780-nm femtosecond laser irradiation, using photoemission electron microscopy (PEEM). By comparing our PEEM observables to finite-difference time-domain simulations, we demonstrate that photoemission from the sub-100-nm structures is enhanced in the region of propagating surface plasmons launched from the nanohole arrays.

DOI: 10.1103/PhysRevApplied.2.064012

Photocathodes convert photons into free electrons that can be readily harnessed for a variety of applications. For example, high-brightness photocathodes are currently used as electron sources in free-electron lasers (FELs) [1], energy-recovery linacs, and inverse-Compton-scattering sources [2]. The light sources employed to initiate the photoemission process range from broadband ultraviolet (UV) lamps to femtosecond (fs) laser sources. Advances in ultrafast laser technology over the past several decades made the generation of fs UV pulses readily feasible, most commonly through harmonic generation. However, due to the inherent inefficiency of higher-harmonic generation, the fundamental laser powers used need to be substantial to produce sufficiently intense electron bunches for the aforementioned applications. A viable alternative comprises the use of ultrafast near-infrared (IR) lasers to directly generate ultrafast electron bunches through nonlinear photoabsorption in metals [3,4]. Indeed, recent reports demonstrate that when compared to UV laser excitation, higher-photoemission intensities can be achieved through multiphoton photoemission driven by IR laser pulses with rather modest energies [5,6].

Metals are prime candidates for photocathode applications because of their high tolerance to intense pulsed laser irradiation. However, metals are typically highly reflective [7] in the near-IR such that light couples poorly into flat metal substrates. With advances in nanofabrication technology, nanostructures such as holes [8], ridges [9], and slits [10] can be easily etched into metal surfaces. These structures can efficiently couple the incident-radiation field [6,11–13] into the metal and generate propagating surface-plasmon eigenmodes [14]. In this regard, surface plasmons can be focused, interfered, and wave-guided [15] using designed nanostructures. Specifically engineered nanostructures can potentially enhance electron photoemission [16] from selectable locations including those remote from the excitation region [17,18]. It is therefore of great interest to explore plasmonic structures in metal surfaces as high-brightness photoemission sources, and as a means to couple and control plasmon propagation. To date, very few studies explore the possibility of using plasmonic constructs [19] as high-brightness photocathodes.

Herein, we describe the fabrication and characterization of nanostructured gold photoemitters which exhibit high-brightness photoemission under femtosecond near-IR laser excitation. The photoemitters consist of nanohole arrays, fabricated using focused-ion-beam (FIB) lithography of a vapor-deposited gold film, and sub-100-nm structures formed during rather gentle subsequent heat treatment. The nanohole-array construct is used to couple IR light into the gold film and launch propagating surface plasmons which further enhance photoemission from the self-assembled metal nanostructures. We measure the relative electron yield as a function of nanohole-array diameter and period. The results are a clear demonstration of the possibility to improve the photoemission of a pure metal using rather simple methods, all in an effort to create high-brightness photoemitters. We compare our experimental observations to finite-difference time-domain (FDTD) calculations.

Metal substrates are prepared by sputtering a 100-nm-thick gold layer on a clean glass substrate. Nanohole arrays (5×5) are etched in the gold film using FIB (FEI QUANTA 3D dual-beam scanning electron microscopy–Ga FIB). Several arrays are fabricated with nanohole diameters varying from 600 to 1000 nm, and periods varying between 1500 and 3000 nm. The samples are subsequently annealed at 200 °C for 2 h under ambient laboratory conditions. The temperature in the furnace is increased from 25 °C to 200 °C within 10 min to avoid the detachment of the gold layer from the glass substrate. Figure 1 is a schematic representation of

*Corresponding author.
wayne.hess@pnnl.gov

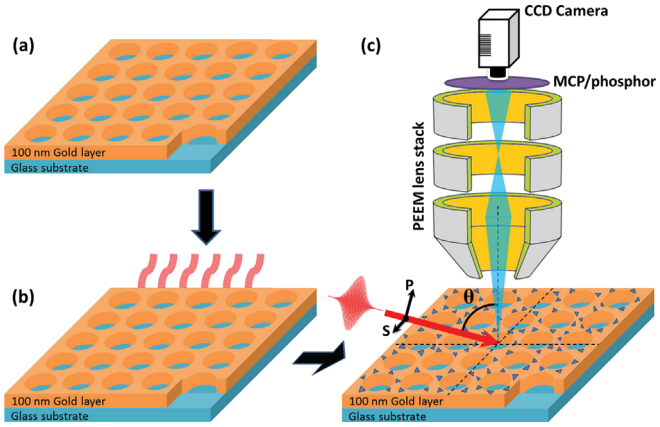

FIG. 1 (a) 100-nm gold thin film is sputtered on a clean glass substrate with nanohole arrays (5 × 5) fabricated by FIB lithography. (b) The sample is then annealed at 200 °C for 2 h in air. (c) The resulting sample is transferred into the PEEM for the photoemission measurement under fs laser irradiation with an incident angle θ = 75°. Schematically illustrated in (c) are *s* and *p* polarization.

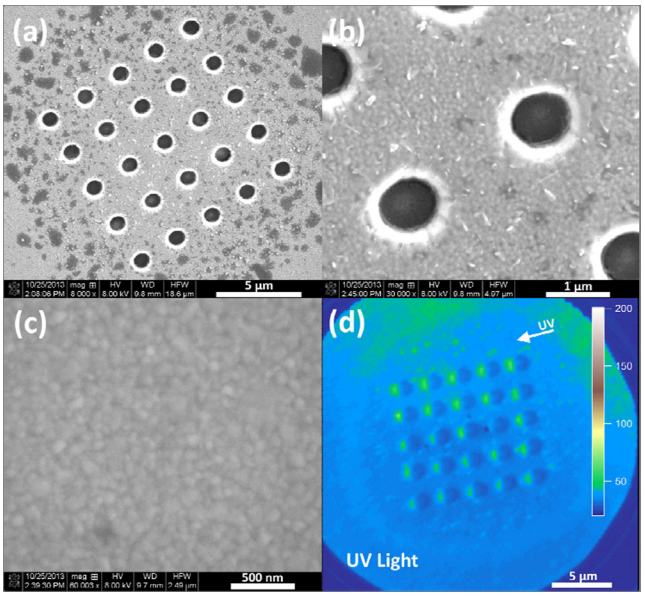

FIG. 2. (a) SEM image of the nanostructured photoemitter which consists of a (5 × 5) nanohole array (1000-nm-diameter holes separated by 2500 nm) fabricated by FIB lithography and heat treated to form nanostructures in the vicinity of the nanoholes within the etched region. These nanostructures only form near the nanohole array, and not on the flat film. (b) Magnified SEM image of the metal nanostructures consisting of nanotips, nanorods, and nanoflakes grown from the gold thin film. (c) Magnified gold surface far from the nanohole array appears identical to the gold thin film prior to heat treatment. (d) PEEM image of the nanostructured photoemitters with 2500-nm nanohole separations and 1000-nm hole diameter illuminated by the UV lamp.

the sample preparation procedure and our experimental apparatus.

Photoemission from the sample surface is imaged by photoemission electron microscopy (PEEM), featuring 20-nm lateral spatial resolution (Elmitec, PEEM III). The sample is mounted approximately 2 mm from an electrically grounded objective lens. A −20 kV electronic potential is applied to the sample in order to accelerate and transfer the photoelectrons to an imaging column containing a series of electromagnetic lenses which focus and project the photoelectron image onto a microchannel plate (MCP) with phosphor screen detector. Images are acquired with a computer-controlled charge-coupled device camera. The base pressure of the microscope chamber is $\sim 9 \times 10^{-11}$ torr.

The sample is irradiated with laser pulses centered at 780 nm from a 90 MHz titanium-sapphire femtosecond oscillator (Griffin-10, KM Labs). Following external-prism pair-compression, transform-limited pulses of ∼12 fs in duration are delivered to the sample chamber. The laser is focused to a $\sim 8 \times 10^{-3}$ mm^2 area, and its polarization is controlled using a half-wave plate, as illustrated schematically in Fig. 1(c). In addition to the femtosecond laser, an unpolarized laser-driven plasma source (UV lamp maximum photon energy $h\nu_{\max} \sim 6.7$ eV) is used to acquire reference single-photon PEEM images.

The FDTD method [20] is used to compute the electromagnetic response of a nanohole array excited by a fs laser pulse. The basic principle of the FDTD method is to numerically solve Maxwell's equations on a finite-element grid representing the designated structure and material [20]. Simulations are performed using a commercially available software package (Lumerical, Inc.) running on a parallel-processor local computer cluster. The computational model replicates the experimental specimen by accounting for sample permittivity, laser wavelength, polarization, and angle of incidence. The calculations incorporate the substrate, gold thin film, and etched holes in a three-dimensional simulation volume using a total field or scattered field source set at a 75° angle of incidence. The source bandwidth is limited by appropriate choice of pulse width in order to limit dispersion in the injection angle. Perfectly matched layer boundary conditions are used in all dimensions to absorb scattered fields. The optical constants for gold are taken from Johnson and Christy [7]. The calculations yield spatially resolved relative intensities of the electric-field components as a function of time. Standard Fourier transformation results in the corresponding spatial- and frequency-resolved relative field magnitudes. These results are directly comparable to the measured PEEM images.

Figure 2 shows the SEM image of a heat-treated (5 × 5) nanohole array on a 100-nm gold film. The diameter of each individual hole is ∼1000 nm and the period is 2500 nm. The postlithography heat treatment induces growth of sub-100-nm structures (nanostructures) localized in the 20 × 20 μm^2 region of the nanohole array. Evidently, the growth of nanostructures is related to the FIB lithographic process, as nanometric structures did not form

away from the etched region of the metal substrate [Fig. 2(c)]. The roughness of the gold film prior to heat treatment is equivalent to that reported for similar gold thin films formed by physical vapor deposition [21]. Under higher magnification, the nanostructures can be better visualized [Fig. 2(b)]. Most nanostructures can be qualitatively described as nanotips, nanorods, or nanoflakes. Due to the sharpness of these nanostructures, strong photoemission following laser illumination is expected [22–26].

The photoemission measurements of nanohole arrays and self-assembled nanostructures are carried out using PEEM. Because of the high-magnification imaging capability, PEEM is ideal for mapping nanoscale photoemission intensities [27]. Figure 2(d) shows the image of a nanohole array with 2500-nm hole separation, recorded following UV-lamp irradiation. The maximum UV photon energy exceeds the work function of gold, therefore the nanohole, nanostructures, and surrounding flat surface exhibit similar photoemission intensity. As such, the observed UV-lamp-generated PEEM image predominantly displays topological contrast in the hole-array region [28].

When illuminated with a 780 nm p-polarized laser, bright photoemission is observed in the nanostructure region surrounding the nanohole array while little photoemission is observed from the adjacent flat surface [Fig. 3(a)]. Although the maximum laser intensity approaches 1 GW/cm^2, the high brightness of the nanostructured photoemitters saturates the PEEM detector at laser powers above 0.09 GW/cm^2. The relative photoemission yield from nanohole arrays prior to heat treatment is more than 10 times weaker than its analog recorded following heat treatment, demonstrating strong photoemission from the nanostructures. Under s-polarized laser illumination, photoemission is very weak, as evidenced from inspection of Fig. 3(b). This observation stresses that the photoemission from the nanometric metal structures is generated by the $\boldsymbol{E}_z$ component (perpendicular to the sample surface) of the enhanced local electric field, whereas the s-polarized light shows weak coupling to the nanohole array. Notice how most of the prominent photoemission spots are found to form striped patterns on the right-hand side of the nanohole array and that the photoemission intensity increases from left to right [Fig. 3(a)].

Previous reports and analyses [12,13] of isolated nanohole and nanohole arrays indicate efficient light coupling into the metal film with the formation of propagating surface plasmons. It appears that the photoemission from the nanostructures is further enhanced in the regions of propagating surface plasmons, and the overall collective "hotspot" pattern traces the surface-plasmon-propagation pattern. For the FDTD simulations, a (5×5) nanohole array etched into a flat gold surface (without nanostructures) is modeled with a 780-nm-wavelength femtosecond light pulse that propagates from left to right, impinging on

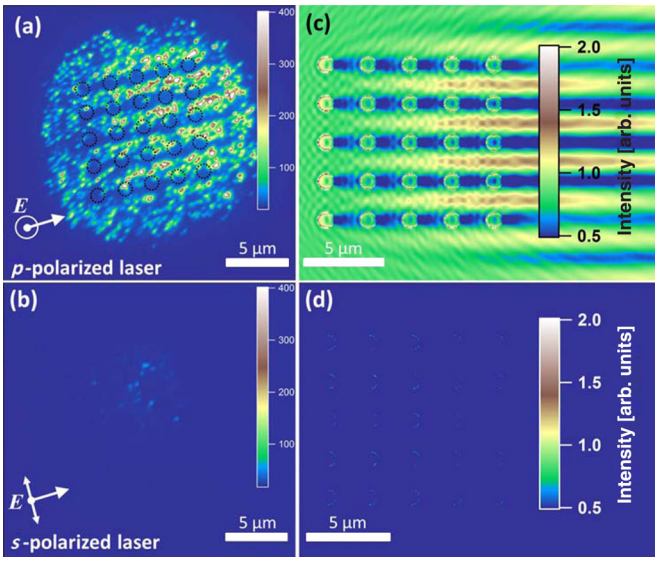

FIG. 3. (a) PEEM image of the nanostructured photoemitters with 2500-nm nanohole separations and 1000-nm hole diameter irradiated by a 780-nm p-polarized laser at 75° from normal. The nanostructures produce strong photoemission with the brightest region always to the right side of the nanohole array, forming a stripe pattern aligned with the laser propagation. Dashed circles indicate hole positions while the arrow indicates the laser propagation direction. The exposure time is 0.15 s. (b) Under illumination of s-polarized light, nanostructured photoemitters show very low photoemission from both the nanostructured and flat surface regions (color bars are in arbitrary units). (c) FDTD calculated electric-field-intensity map for a 5×5 nanohole array etched in a gold film irradiated by a 780-nm fs laser pulse. The plane wave is polarized with electric vector parallel to the out-of-plane axis (p polarization). (d) FDTD simulation of the nanohole array with s-polarized laser pulse. The laser pulse propagates from left to right in both simulations.

the sample at a 75° angle of incidence. The field enhancement (E/E_{incident}) calculated by FDTD for the array under p and s polarization is displayed in Figs. 3(c) and 3(d). Under p-polarized laser excitation, high field enhancement is evident between the nanohole rows on the right side of the array. The simulation reveals that the highly enhanced local field regions interfere to form a striped oscillating intensity pattern propagating beyond the hole array. The PEEM image indicates that photoexcitation of the metal interface occurs through the generation of surface plasmons. The combination of propagating plasmons and laser field leads to the characteristic emission pattern observed in Fig. 3(a). FDTD simulations of the hole structures, composed of different hole diameters and separation distances, produce results that compare well with the analogous experimental images. Namely, the regions of field enhancement qualitatively match the electron photoemission map and intensity, thus validating our premise that the highest photoemission occurs in regions where there is overlap of the metal nanostructures with propagating surface plasmons. Moreover, the simulations reveal that the field enhancement

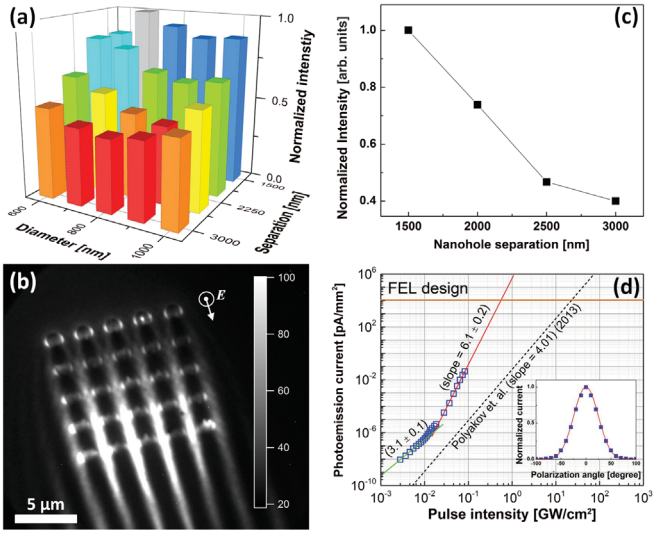

FIG. 4. (a) Normalized photoemission intensity for nanostructured photoemitters plotted as a function of nanohole diameter and separation. The photoemission intensity increases modestly when the separation between nanoholes decreases from 3000 nm to 1500 nm. (b) PEEM image of a nanohole array (separation and hole diameter of 2500 and 1000 nm respectively) without self-assembled nanostructure (no heat treatment). (c) Nanohole-separation dependence of normalized photoemission intensity for nanohole arrays without self-assembled nanostructure. The trend apparent in (a) is consistent with the results in (c). (d) Photoemission current is plotted as a function of laser intensity for the self-assembled nanostructure photoemitter on a log-log scale. Three-photon absorption process is observed (green line) under low laser intensity; however, under high laser intensity (red line), the data yield a sixth-order photoemission scaling. The inset shows the polarization dependence of the photoemission intensity measured in the region of high laser intensity where 0° represents p polarization. Dashed line shows power dependence of a gold nanograting photoemitter (Polyakov *et al.* [6]).

throughout the surface is extremely weak following s-polarized laser illumination, which again parallels our experimental observations [Figs. 3(b) and 3(d)].

Figure 4(a) displays the normalized photoemission yield as a function of nanohole-array geometry, for 20 different combinations of hole diameters and separations. The normalized photoemission intensity increases modestly (by a factor of 2) when the nanohole-array separation decreases from 3000 nm to 1500 nm. This trend of increased photoemission intensity as separation distance is decreased is paralleled in PEEM measurements of nanohole arrays without the self-assembled nanostructures [Fig. 4(c)]. In this regard, a PEEM image of a nanohole array without self-assembled nanostructures is displayed in Fig. 4(b) for comparison.

Figure 4(d) displays the relative photoemission current as a function of laser intensity in a log-log plot, measured from an array with hole separations and diameters of 2500 and 1000 nm, respectively. Based on Fowler-Dubridge theory [29,30], the multiphoton photoemission current density is proportional to the nth power of the laser intensity such that photoemission intensity scales with the laser power density as

$$I_n \propto P^n,$$

where I_n is the photoemission intensity defined as the average intensity over the photoemitter area and P is the laser power density. The nonlinear photoemission intensity does not follow this relation as a function of laser intensity, but rather displays two distinct regimes of "low-" and "high-" intensity responses. At low intensities (below 0.01 GW/cm^2) three-photon absorption ($n = 3.1$) is indicated (green solid line). This is what would be expected based on the photon energy used (1.59 eV) and the work function of gold (~4.5 eV). At high intensities, however, (above 0.02 GW/cm^2) the line fit gives $n = 6.1 \pm 0.2$, which indicates a highly nonlinear six-photon process (red solid line). It is worth mentioning that both nanohole arrays and the self-assembled nanostructures appear to be robust, showing no indication of laser-induced ripening, melting, ablation, or decrease in photoemission intensity even after prolonged illumination at high laser power (~1 GW/cm^2).

Assuming the P^6 dependence holds at an irradiance of ~1 GW/cm^2, then the brightness of the device proposed here can achieve the requirement of future FEL designs [6,31] with the laser intensity remaining below the ablation threshold of gold [32]. The photoemission yield measured as a function of laser polarization (measured using the high-laser-intensity data) is shown in the inset of Fig. 4(d). The result can be fitted to $I(\theta) \propto [\cos^2\theta]^6$, as expected for a six-photon process. Although three-photon emission is typically observed from gold substrates [33], there are reports of highly nonlinear multiphoton emission processes, including $n = 4$ for gold nanocavity arrays [6], $n = 4.5$ for gold pads [34], $n = 5$ for sharp gold nanotips [25], and $n = 5.5$ for gold nanoparticles [35]. Observations of highly nonlinear photoemission have been attributed to an enhanced contribution from high-density states below the Fermi level [25] and the advent of field emission due to strong near-field enhancement of laser excited localized surface plasmons [35].

Overall, our results suggest that the combination of nanohole arrays and nanostructured surfaces could serve as high-brightness electron sources. For example, while thermionic cathodes remain the electron sources of choice for many accelerators [31], next-generation light sources, including FELs and synchrotron designs, will be based on bright and directed pulsed electron sources. It appears promising that metal nanostructured photoemission sources could be applied in FEL designs using laser pulses with intensities well below the metal's ablation threshold [32]. Moreover, with modern physical and chemical techniques such as holographic lithography [36,37], it is straightforward to fabricate relatively large-scale nanohole arrays with

tunable diameters and separations, or other periodic plasmonic nanostructures, thereby allowing a more flexible design of tailored photoemission sources.

In summary, we demonstrate high-brightness photoemission from gold nanohole arrays featuring rodlike nanoscale structures fabricated by a combination of FIB lithography followed by heat treatment. The photoemission from self-assembled sub-100-nm structures is enhanced in the region of propagating surface plasmons launched from light coupled into the nanohole array. This conclusion is supported by FDTD simulations of nanohole arrays that display striped electric field patterns following pulsed fs excitation. The intensity ratio of photoemission from the nanostructured gold to the flat metal surface can be as high as 10^8 at a modest laser intensity of 1.0 GW/cm^2. The reported constructs are promising candidates for applications requiring high-brightness photoemission sources.

This work was supported by the U. S. Department of Energy, Office of Science, Office of Basic Energy Sciences, Division of Chemical Sciences, Geosciences and Biosciences. Pacific Northwest National Laboratory (PNNL) is a multiprogram national laboratory operated for DOE by Battelle. P. Z. E. acknowledges support from the Laboratory Directed Research and Development Program through a Linus Pauling program at PNNL. L. M. K. was supported by the Chemical Imaging Initiative conducted under the Laboratory Directed Research and Development plan at PNNL. This work was performed using EMSL, a national scientific user facility sponsored by the Department of Energy's Office of Biological and Environmental Research and located at PNNL.

[1] W. Ackermann *et al.*, Operation of a free-electron laser from the extreme ultraviolet to the water window, Nat. Photonics **1**, 336 (2007).

[2] W. S. Graves, F. X. Kartner, D. E. Moncton, and P. Piot, Intense superradiant X rays from a compact source using a nanocathode array and emittance exchange, Phys. Rev. Lett. **108**, 263904 (2012).

[3] D. H. Dowell, I. Bazarov, B. Dunham, K. Harkay, C. Hernandez-Garcia, R. Legg, H. Padmore, T. Rao, J. Smedley, and W. Wan, Cathode R&D for future light sources, Nucl. Instrum. Methods Phys. Res., Sect. A **622**, 685 (2010).

[4] P. Musumeci, J. T. Moody, R. J. England, J. B. Rosenzweig, and T. Tran, Experimental generation and characterization of uniformly filled ellipsoidal electron-beam distributions, Phys. Rev. Lett. **100**, 244801 (2008).

[5] P. Musumeci, L. Cultrera, M. Ferrario, D. Filippetto, G. Gatti, M. S. Gutierrez, J. T. Moody, N. Moore, J. B. Rosenzweig, C. M. Scoby, G. Travish, and C. Vicario, Multiphoton photoemission from a copper cathode illuminated by ultrashort laser pulses in an rf photoinjector, Phys. Rev. Lett. **104**, 084801 (2010).

[6] A. Polyakov, C. Senft, K. F. Thompson, J. Feng, S. Cabrini, P. J. Schuck, H. A. Padmore, S. J. Peppernick, and W. P. Hess, Plasmon-enhanced photocathode for high brightness and high repetition rate x-ray sources, Phys. Rev. Lett. **110**, 076802 (2013).

[7] P. B. Johnson and R. W. Christy, Optical constants of noble metals, Phys. Rev. B **6**, 4370 (1972).

[8] L. Yin, V. K. Vlasko-Vlasov, A. Rydh, J. Pearson, U. Welp, S. H. Chang, S. K. Gray, G. C. Schatz, D. B. Brown, and C. W. Kimball, Surface plasmons at single nanoholes in au films, Appl. Phys. Lett. **85**, 467 (2004).

[9] J. A. Sanchez-Gil and A. A. Maradudin, Surface-plasmon polariton scattering from a finite array of nanogrooves/ridges: Efficient mirrors, Appl. Phys. Lett. **86**, 251106 (2005).

[10] K. G. Lee and Q. H. Park, Coupling of surface plasmon polaritons and light in metallic nanoslits, Phys. Rev. Lett. **95**, 103902 (2005).

[11] A. Kubo, Y. S. Jung, H. K. Kim, and H. Petek, Femtosecond microscopy of localized and propagating surface plasmons in silver gratings, J. Phys. B **40**, S259 (2007).

[12] Y. Gong, A. G. Joly, P. Z. El-Khoury, and W. P. Hess, Nonlinear photoemission electron micrographs of plasmonic nanoholes in gold thin films, J. Phys. Chem. C **118**, 25671 (2014).

[13] Y. Gong, A. G. Joly, P. Z. El-Khoury, and W. P. Hess, Interferometric plasmonic lensing with nanohole arrays, J. Phys. Chem. Lett. **5**, 4243 (2014).

[14] A. Kubo, N. Pontius, and H. Petek, Femtosecond microscopy of surface plasmon polariton wave packet evolution at the silver/vacuum interface, Nano Lett. **7**, 470 (2007).

[15] W. L. Barnes, A. Dereux, and T. W. Ebbesen, Surface plasmon subwavelength optics, Nature (London) **424**, 824 (2003).

[16] S. J. Peppernick, A. G. Joly, K. M. Beck, and W. P. Hess, Near-field focused photoemission from polystyrene microspheres studied with photoemission electron microscopy, J. Chem. Phys. **137**, 014202 (2012).

[17] Y. Wang, X. J. Liu, D. Whitmore, W. D. Xing, and E. O. Potma, Remote multi-color excitation using femtosecond propagating surface plasmon polaritons in gold films, Opt. Express **19**, 13454 (2011).

[18] P. Berini, Long-range surface plasmon polaritons, Adv. Opt. Photonics **1**, 484 (2009).

[19] R. K. Li, H. To, G. Andonian, J. Feng, A. Polyakov, C. M. Scoby, K. Thompson, W. Wan, H. A. Padmore, and P. Musumeci, Surface-plasmon resonance-enhanced multiphoton emission of high-brightness electron beams from a nanostructured copper cathode, Phys. Rev. Lett. **110**, 074801 (2013).

[20] A. Taflove and S. C. Hagness, *Computational Electrodynamics: The Finite-Difference Time Domain Method* (Artech, Boston, 2005).

[21] M. Melli, A. Polyakov, D. Gargas, C. Huynh, L. Scipioni, W. Bao, D. F. Ogletree, P. J. Schuck, S. Cabrini, and A. Weber-Bargioni, Reaching the theoretical resonance quality factor limit in coaxial plasmonic nanoresonators fabricated by helium ion lithography, Nano Lett. **13**, 2687 (2013).

[22] M. Schenk, M. Kruger, and P. Hommelhoff, Strong-field above-threshold photoemission from sharp metal tips, Phys. Rev. Lett. **105**, 257601 (2010).

[23] R. Ganter, R. Bakker, C. Gough, S. C. Leemann, M. Paraliev, M. Pedrozzi, F. Le Pimpec, V. Schlott, L. Rivkin, and A. Wrulich, Laser-photofield emission from needle cathodes for low-emittance electron beams, Phys. Rev. Lett. **100**, 064801 (2008).

[24] S. Tsujino, P. Beaud, E. Kirk, T. Vogel, H. Sehr, J. Gobrecht, and A. Wrulich, Ultrafast electron emission from metallic nanotip arrays induced by near infrared femtosecond laser pulses, Appl. Phys. Lett. **92**, 193501 (2008).

[25] R. Bormann, M. Gulde, A. Weismann, S. V. Yalunin, and C. Ropers, Tip-enhanced strong-field photoemission, Phys. Rev. Lett. **105**, 147601 (2010).

[26] P. Dombi, A. Horl, P. Racz, I. Marton, A. Trugler, J. R. Krenn, and U. Hohenester, Ultrafast strong-field photoemission from plasmonic nanoparticles, Nano Lett. **13**, 674 (2013).

[27] S. Anders, H. A. Padmore, R. M. Duarte, T. Renner, T. Stammler, A. Scholl, M. R. Scheinfein, J. Stohr, L. Seve, and B. Sinkovic, Photoemission electron microscope for the study of magnetic materials, Rev. Sci. Instrum. **70**, 3973 (1999).

[28] G. Xiong, R. Shao, S. J. Peppernick, A. G. Joly, K. M. Beck, W. P. Hess, M. Cai, J. Duchene, J. Y. Wang, and W. D. Wei, Materials applications of photoelectron emission microscopy, JOM **62**, 90 (2010).

[29] R. H. Fowler, The analysis of photoelectric sensitivity curves for clean metals at various temperatures, Phys. Rev. **38**, 45 (1931).

[30] L. A. DuBridge, Theory of the energy distribution of photoelectrons, Phys. Rev. **43**, 0727 (1933).

[31] W. A. Barletta *et al.*, Free electron lasers: Present status and future challenges, Nucl. Instrum. Methods Phys. Res., Sect. A **618**, 69 (2010).

[32] L. Torrisi, G. Ciavola, S. Gammino, L. Ando, A. Barna, L. Laska, and J. Krasa, Metallic etching by high power Nd: Yttrium-aluminum-garnet pulsed laser irradiation, Rev. Sci. Instrum. **71**, 4330 (2000).

[33] E. M. Logothetis and P. L. Hartman, Laser-induced electron emission from solids: Many-photon photoelectric effects and thermionic emission, Phys. Rev. **187**, 460 (1969).

[34] V. Schweikhard, A. Grubisic, T. A. Baker, and D. J. Nesbitt, Multiphoton scanning photoionization imaging microscopy for single-particle studies of plasmonic metal nanostructures, J. Phys. Chem. C **115**, 83 (2011).

[35] F. Schertz, M. Schmelzeisen, M. Kreiter, H. J. Elmers, and G. Schonhense, Field emission of electrons generated by the near field of strongly coupled plasmons, Phys. Rev. Lett. **108**, 237602 (2012).

[36] M. Campbell, D. N. Sharp, M. T. Harrison, R. G. Denning, and A. J. Turberfield, Fabrication of photonic crystals for the visible spectrum by holographic lithography, Nature (London) **404**, 53 (2000).

[37] F. Y. Lee, K. H. Fung, T. L. Tang, W. Y. Tam, and C. T. Chan, Fabrication of gold nano-particle arrays using two-dimensional templates from holographic lithography, Curr. Appl. Phys. **9**, 820 (2009).